Article

TRANSPARENT PROCESS

THE EMBO JOURNAL

# Whole chromosome loss and associated breakage–fusion–bridge cycles transform mouse tetraploid cells

Rozario Thomas[1,2], Daniel Henry Marks[2], Yvette Chin[2] & Robert Benezra[1,2,*]

## Abstract

**Whole chromosome gains or losses (aneuploidy) are a hallmark of ~70% of human tumors. Modeling the consequences of aneuploidy has relied on perturbing spindle assembly checkpoint (SAC) components, but interpretations of these experiments are clouded by the multiple functions of these proteins. Here, we used a Cre recombinase-mediated chromosome loss strategy to individually delete mouse chromosomes 9, 10, 12, or 14 in tetraploid immortalized murine embryonic fibroblasts. This methodology also involves the generation of a dicentric chromosome intermediate, which subsequently undergoes a series of breakage–fusion–bridge (BFB) cycles. While the aneuploid cells generally display a growth disadvantage *in vitro*, they grow significantly better in low adherence sphere-forming conditions and three of the four lines are transformed *in vivo*, forming large and invasive tumors in immunocompromised mice. The aneuploid cells display increased chromosomal instability and DNA damage, a mutator phenotype associated with tumorigenesis *in vivo*. Thus, these studies demonstrate a causative role for whole chromosome loss and the associated BFB-mediated instability in tumorigenesis and may shed light on the early consequences of aneuploidy in mammalian cells.**

**Keywords** aneuploidy; chromosomal instability; chromosome losses; tetraploidy; tumorigenesis

**Subject Categories** Cancer; Cell Cycle

**DOI** 10.15252/embj.201797630 | Received 20 June 2017 | Revised 25 October 2017 | Accepted 7 November 2017 | Published online 1 December 2017

**The EMBO Journal (2018) 37: 201–218**

## Introduction

While aneuploidy is associated with a high percentage of human cancers, whether it can directly promote tumorigenesis is still not firmly established. Most current models of aneuploidy rely on altering the levels of various SAC proteins, which ensure sister chromatid segregation occurs only after chromosomes are properly bi-oriented during metaphase. Several mouse models of aneuploidy have been generated that harbor hypomorphic alleles or heterozygous knockouts for key SAC proteins such as Mad2, Bub3, and BubR1 with varying tumor penetrance, spectrum and latency (Schvartzman *et al*, 2010; Simon *et al*, 2015). However, genetic loss of these SAC components is not usually observed in human tumors. In contrast, SAC components are frequently overexpressed. For instance, Mad2, a key SAC protein is overexpressed in a wide array of human tumors, and in transgenic mouse models, overexpression of Mad2 can initiate and promote tumorigenesis (Sotillo *et al*, 2007). A major caveat of these mouse models is that SAC proteins have other non-mitotic functions such as in nuclear trafficking, transcriptional repression, apoptosis and the DNA damage response (Schvartzman *et al*, 2010). Therefore, it is unclear whether the pro-tumor phenotype observed is a direct result of the aneuploidy generated.

Other groups have generated yeast, mouse and human cells with single chromosome gains. Haploid yeast strains harboring extra chromosomes exhibit a growth disadvantage compared to the controls and a transcriptional response similar to the yeast environmental stress response (Torres *et al*, 2007). Also, the growth inhibitory phenotypes of these disomic strains were due to the expression of the genes present on the extra chromosome and on the stoichiometric imbalance resulting from the supernumerary proteins (Torres *et al*, 2007). The aneuploid cells adapt by buffering the levels of these extra proteins and are therefore more sensitive to additional proteotoxic stress, like inhibitors of protein folding and protein degradation (Torres *et al*, 2007; Oromendia *et al*, 2012). In addition, these aneuploid strains were also found to lose other chromosomes at a high frequency and to exist in a generally unstable karyotypic state (Sheltzer *et al*, 2011).

Experiments using trisomic mouse embryonic fibroblasts (MEFs) have shown that they also have growth impairment relative to the euploid MEFs and a delay in the rate to spontaneously immortalize (Williams *et al*, 2008). The growth impairment has been attributed to the proteotoxic stress associated with carrying the extra chromosomes. Similar to the yeast model, these trisomic MEFs have been shown to be sensitive to proteotoxic stressors since their protein folding and degradation machinery is already under duress (Tang *et al*, 2011). Also, in reconstitution experiments into lethally

1 BCMB Program, Weill Cornell Graduate School of Medical Sciences (WCGSMS), New York, NY, USA
2 Cancer Biology and Genetics Program, Memorial Sloan Kettering Cancer Center (MSKCC), New York, NY, USA
*Corresponding author. Tel: +1 646 888 2812; E-mail: r-benezra@ski.mskcc.org

irradiated mouse recipients, these trisomic hematopoietic stem cells (HSCs) displayed reduced fitness in comparison with the wild-type HSCs (Pfau *et al*, 2016). The fitness and neoplastic defects in the trisomic MEFs are not overcome even with the addition of oncogenic mutations (Sheltzer *et al*, 2017). Recently, trisomic mouse embryonic stem (ES) cells were generated by a series of steps involving random integration of a dual drug selection cassette followed by expansion in culture to allow for an increase in copy number and finally Cre recombination to generate dual drug-resistant ES cells, trisomic for a particular chromosome. These trisomic ES cells were found to be less differentiated and have enhanced teratoma forming potential in comparison with the wild-type ES cells (Zhang *et al*, 2016).

Human cells harboring extra chromosome(s) have a similar growth defect and exhibit a uniform aneuploidy response signature (specific pathways being up-regulated or down-regulated irrespective of the identity of the chromosome gained; Stingele *et al*, 2012). Interestingly, while the DNA and mRNA copy numbers are increased corresponding to the specific chromosome gained, the protein levels, especially those that are subunits of multi molecular complexes, are maintained at normal levels. One way these trisomic or tetrasomic aneuploid cells achieve this protein homeostasis is by increasing the function of the autophagy pathway (Stingele *et al*, 2012). Also, human cells with extra chromosomes were shown to have replicative defects because of down-regulation of the helicase, MCM2-7, and importantly, these aneuploid cells were found to be genomically unstable (Passerini *et al*, 2016). Similar experiments on trisomic colorectal cancer cells also show that these aneuploid cells mis-segregate chromosomes at a higher rate than the control diploids (Nicholson *et al*, 2015).

While all of the studies mentioned above focus on gain of chromosome aneuploidies, to our knowledge, no groups have studied the effects of chromosome-loss-mediated aneuploidy on cellular fitness and tumorigenesis. Furthermore, a comprehensive study of human tumor karyotypes revealed a strong disposition for chromosome loss rather than gains (Duijf *et al*, 2013). Here, we show that a combination of losing individual chromosomes and a series of breakage–fusion–bridge (BFB) cycles in a tetraploid background induces further genetic instability and drives tumorigenesis in a mouse allograft model.

## Results

### Generation of Cre recombinase-mediated whole chromosome loss

In order to model chromosome loss events, we generated SV40 large T antigen immortalized MEFs bearing a pair of inverted loxP sites (iLoxP) on one homolog of chromosome 9, 10, 12, or 14 (Ch9, Ch10, Ch12, or Ch14; Fig 1A). As reported in other studies, these MEFs become tetraploid as a result of the large T antigen immortalization procedure (Hein *et al*, 2009; Lionnet *et al*, 2011), and thus, the initial ploidy prior to any experimentation on these MEFs is 4N. Upon Cre expression, recombination between the duplicated sister chromatids yields either the same parental configuration or an inverted recombination to yield a pair of acentric and dicentric fragments (Fig 1B). The acentric fragments are not maintained during repeated cell divisions and the dicentric fragments undergo BFB cycles in subsequent mitoses and are eventually lost (Zhu *et al*, 2010). Since the iLoxP sites bear an externally flanking surface marker (human Cluster of Differentiation 2—hCD2), all inverted recombination events were assessed by the loss of this marker and cells were sorted by flow cytometry to obtain hCD2 Plus (parental controls) and hCD2 Minus (targeted chromosome loss) populations (Fig 1B and C). For brevity, we refer to cells with engineered chromosome loss events as ICLs (cells with induced chromosome losses) and their unrearranged parental counterparts as controls. While there is a slight increase in the side scatter of the 4OHT-treated cells, this phenomenon was not observed uniformly in all the FACS experiments and we therefore attribute it to batch variations in the FACS setup (Appendix Fig S1A). Previous adaptation of this strategy, in the context of studying loss of heterozygosity (LOH), has shown that recombination-mediated marker loss also correlated strongly with chromosome loss in the lymphoid system in mice (Zhu *et al*, 2010), suggesting that marker loss is a faithful measure of the predicted chromosome loss event both *in vitro* and *in vivo*.

### Validation and tumorigenic potential of early passage aneuploid cells generated by Cre recombination

In order to demonstrate that the expected chromosome loss event took place after Cre-mediated recombination and prior to any/extensive *in vitro* expansion of the sorted cells, we performed low pass whole-genome sequencing (WGS) directly on the FACS sorted ICL and control cells (without any *in vitro* culturing after the sort). As shown in Fig 1D, in each of the four chromosome lines sequenced, compared to the respective control lines, the ICL lines harbored a notable copy number reduction only in the corresponding targeted chromosomes. The absolute *Z*-score, a measure of the number of standard deviations from the mean, was greater than 1, only for the targeted chromosomes in all the ICL lines. The Ch14, Ch9, and Ch10 ICL lines harbored a strong copy number reduction in the distal portions of the corresponding targeted chromosomes. This can be explained by the fact that the hCD2 marker (used to FACS sort), which is present on the distal portion on the chromosome (Fig 1A), is lost initially, followed by additional rounds of BFB cycles in subsequent cell cycles. Accordingly, when the ICL (and the control cells) are expanded further in culture for subsequent experiments (see next section), we observe that portions along the entire length of chromosomes 14 and 9 appear to have been lost in Ch14 and Ch9 ICLs, respectively (Fig EV3). Ch10 ICL cells, upon further expansion, displayed a loss only in the central portion of chromosome 10 (Fig EV3; discussed in next section). The break points at the distal portions of all four ICL lines corresponded accurately with the location of the iLoxP sites on the respective chromosomes (Appendix Fig S1B).

We also obtained similar results on performing WGS on the sorted ICL and control cells after minimal *in vitro* passaging. Only the targeted chromosome exhibited notable copy number reduction (Fig 2A), and the absolute *Z* score was greater than 1, only for the targeted chromosomes in all the ICL lines. Chromosome 7 exhibited a minor, non-significant change in the Ch14 and Ch9 ICL lines. However, in this experiment, we observed only a small copy number change in chromosome 10 in the Ch10 ICL, which can be

 

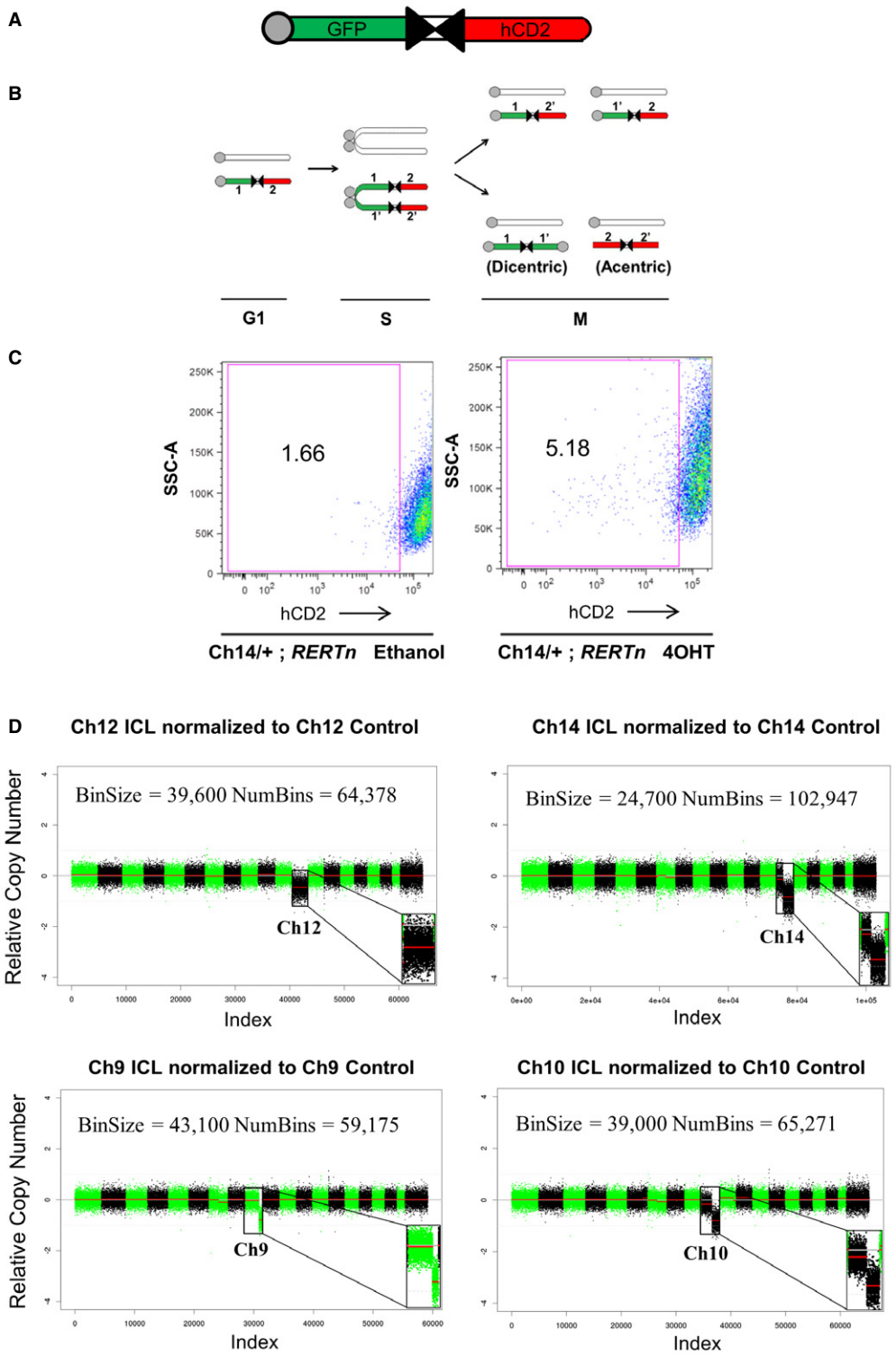


**Figure 1. Generation of ICL in MEFs by Cre recombination.**

A Schematic of the inverted lox P (iLoxP) site, flanked by sortable GFP and hCD2 markers.

B Model of reciprocal recombination yielding parental configurations 1/2′ and 1′/2 and dicentric/acentric configurations as a result of inverted recombination yielding configurations 1/1′ and 2/2′.

C Representative FACS plot showing loss of hCD2 marker expression of Ch14 ICL MEFs after treatment with 4-hydroxy tamoxifen (4OHT) for 14 days to induce Cre, compared to ethanol-treated control cells (See also Appendix Fig S1A).

D Shallow whole-genome sequencing (copy number profiles) of large T antigen immortalized MEFs after exposure to Cre recombinase and sorted for control (hCD2 Plus) and ICL (hCD2 Minus) cells for chromosomes 12, 14 and 9 and 10, without any *in vitro* culturing, post-FACS sort.

attributed to the stochastic nature and frequency of the recombination events in the different chromosomal lines at early time points. Since the populations analyzed were sorted solely for the presence or absence of the hCD2 marker, we anticipated at very low passage numbers very few differences outside the ICL event would be observed. Indeed, as shown in Fig 2A, compared to the control cells, complete loss (Ch12) or distal loss (Ch9, Ch10 and Ch14) of the targeted chromosome was the only prominent event in the ICL cells.

All four of these low passage ICL lines were injected into immunocompromised, athymic nude mice to determine the tumorigenic potential compared to the control populations. In two of the four chromosome lines tested (Ch9 and Ch14), the ICL cells showed dramatic enhancement of tumorigenic potential (Fig 2B). Importantly, neither of these ICL lines showed enhanced growth potential *in vitro*, suggesting that the advantages conferred on the ICL cells are manifested only in certain contexts, such as the stressed environment in the mice (Appendix Fig S2). Thus, our Cre-recombination-mediated strategy was robust in generating the loss of the targeted chromosomes in MEFs, and in two out of four early passage ICL lines, the targeted loss of the distal portions of chromosomes 9 and 14 is largely sufficient to promote tumor formation in nude mice. It should be noted that the loss of distal portion of chromosomes 9 and 14 eventually leads to losses across the entire lengths of these chromosomes in late passage MEFs (see next section).

### Characterization, tumorigenic potential and *in vitro* growth properties of later passage ICL cells

Prior to all subsequent experiments, the immortalized MEFs were sorted three times, serially, to improve the purity of hCD2 Plus (control) and hCD2 Minus (ICL) populations. As anticipated for tetraploid cells lacking pocket protein activity, whole chromosome gains and losses were increased during serial passaging both in the ICL and control cell lines. Importantly, karyotyping analysis of these "later passage" MEFs indicated that all ICL lines showed significant levels of target chromosome loss in 70–80% of the cells (Figs 3 and 4, and EV1; Table 1). Many of the non-targeted chromosomal aberrations (deviations from a copy number of 4) observed in the parental control cells are also found in the respective ICL lines, indicating that the control and ICL lines suffer some common changes that may result from cell passage pressures (see arrows and asterisks in Fig 3A–D). Loss of the target chromosome was by far the most prevalent change in the ICL cells (~80% of the metaphases; Figs 4 and EV1, and Table 1). It should be noted that while a biological replicate of Ch9 ICL harbored a significant copy number change in chromosome 4 (Fig 4A–D), another replicate that was karyotyped did not harbor this chromosome 4 aberration (Fig EV1), suggesting that this change was specific to this replicate. Similarly, significant changes in copy number of a non-targeted chromosome in any of the ICL lines were not consistently observed among biological replicates (Figs 4 and EV1). Significant non-targeted ICL chromosome changes were also not commonly present across the ICLs of various chromosomes (Table 1). Taken together, these results show that the only consistent change that was occurring in all the ICL lines (including replicates of a given chromosome line and different chromosome lines) was the copy number change in the respective targeted chromosomes.

In order to determine whether passaging influenced the tumorigenic potential of these later passage lines, we repeated the xenograft transplantation experiments into immunocompromised mice. ICL lines for Ch9 and Ch14 retained their tumorigenic potential and ICL for Ch10 now gained tumorigenic potential as well (Fig 5A). ICL lines (Ch9, 10, and 14) formed large tumors, which exhibited pronounced neural, muscular and vascular invasiveness, whereas controls either did not grow at all (Ch9) or formed small, non-invasive lesions (Ch10 and 14; Fig 5A and B). This result was corroborated for the Ch10 and Ch14 lines, in the more fully immunodeficient NOD/SCID mouse model, to rule out any immune component to the failure of control cells to form tumors (Fig 5C). Tumors derived from ICL lines still had < 4 copies of the targeted chromosome in ~85% of the cells karyotyped (Fig EV2). In addition to the targeted chromosome losses, these explanted tumor cells also harbored additional non-targeted chromosomal aberrations (Fig EV2), suggesting that these cells were scrambling their karyotype *in vivo*, following the initial targeted chromosome loss.

Also, similar to the no-passage postsort and the minimally passaged early passage MEFs, we also performed shallow WGS on the late passage MEFs to obtain a global snapshot of all the chromosomal changes and aberrations at this later time point. While only distal portions are lost in the WGS of the early passage MEFs, in the late passage MEFs, portions along the entire length of chromosomes 9 and 14 appear to have been lost (Fig EV3). Ch12 ICLs, similar to the earlier WGS results, displayed a copy number loss along the entire length of chromosome 12 (Fig EV3). In late passage Ch10 ICL however, only the central portion of chromosome 10 is lost (Fig EV3). The most likely explanation is, after initial distal chromosome 10 loss, during subsequent passaging, chromosome 10 may be subjected to a series of chromosomal rearrangements and copy number changes leading to specific depletion of the central region. In addition, we observed aberrant copy number profiles of other non-targeted chromosomes like chromosomes 4, 6, 12, etc. Irrespective of these downstream aberrations at later passage, we are confident that copy number changes in the targeted chromosome were the first event and the additional genomic redistributions are secondary to the original event. Importantly, these subsequent events likely contribute to the acquisition of transforming potential of induced chromosome 10 loss.

There are multiple reasons that we attribute the tumor phenotype we observe to copy number variations in the targeted chromosome and not to other sporadic basal chromosome variations in these cells. First, in WGS of our early passage MEFs, the only prominent, initial aneuploidy event that partitioned with the tumor promoting phenotype was the reduction in the copy number of the targeted chromosome in the ICL lines (Fig 2). Second, since each ICL line and matched control was derived from a common MEF line, most of the non-targeted chromosome variations were present in both the ICL and the controls (Figs 3, 4, and EV1; Table 1). Also, unlike the non-targeted chromosomal variations, the targeted chromosome losses in the ICL lines were the most penetrant events occurring in about 70–80% of the ICL cells. Third, there was no clonal selection for any other predominant chromosomal abnormality during the course of tumor formation (data not shown). Finally, similar results were obtained when the experiments were performed using different MEF lines (2–3 biological replicates) for any given ICL chromosome, and we observed the pro-tumorigenic phenotype for three different

 

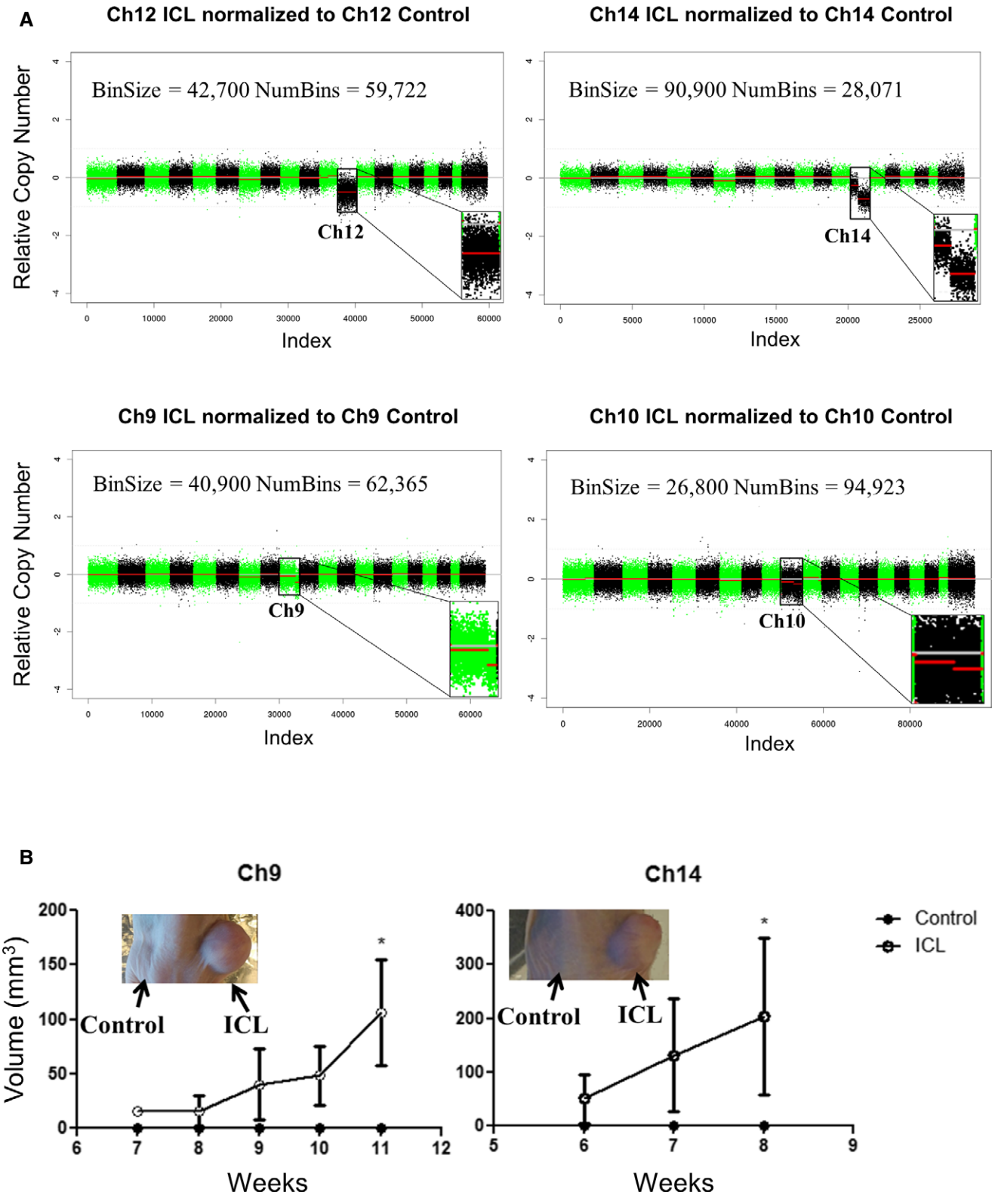


**Figure 2. Validation and tumorigenic potential of early passage aneuploid cells.**

A Shallow whole-genome sequencing (copy number profiles) of large T antigen immortalized, early passage MEFs after exposure to Cre recombinase and sorted for control (hCD2 Plus) and ICL (hCD2 Minus) cells for chromosomes 12, 14 and 9 and 10.

B Tumor growth curve after early passage ICL cells were injected into flanks of athymic nude mice ($n$ = 5 per group and error bars denote SEM, *$P < 0.05$ for Ch9 and Ch14). Two-tailed unpaired $t$-test was used to determine statistical significance.

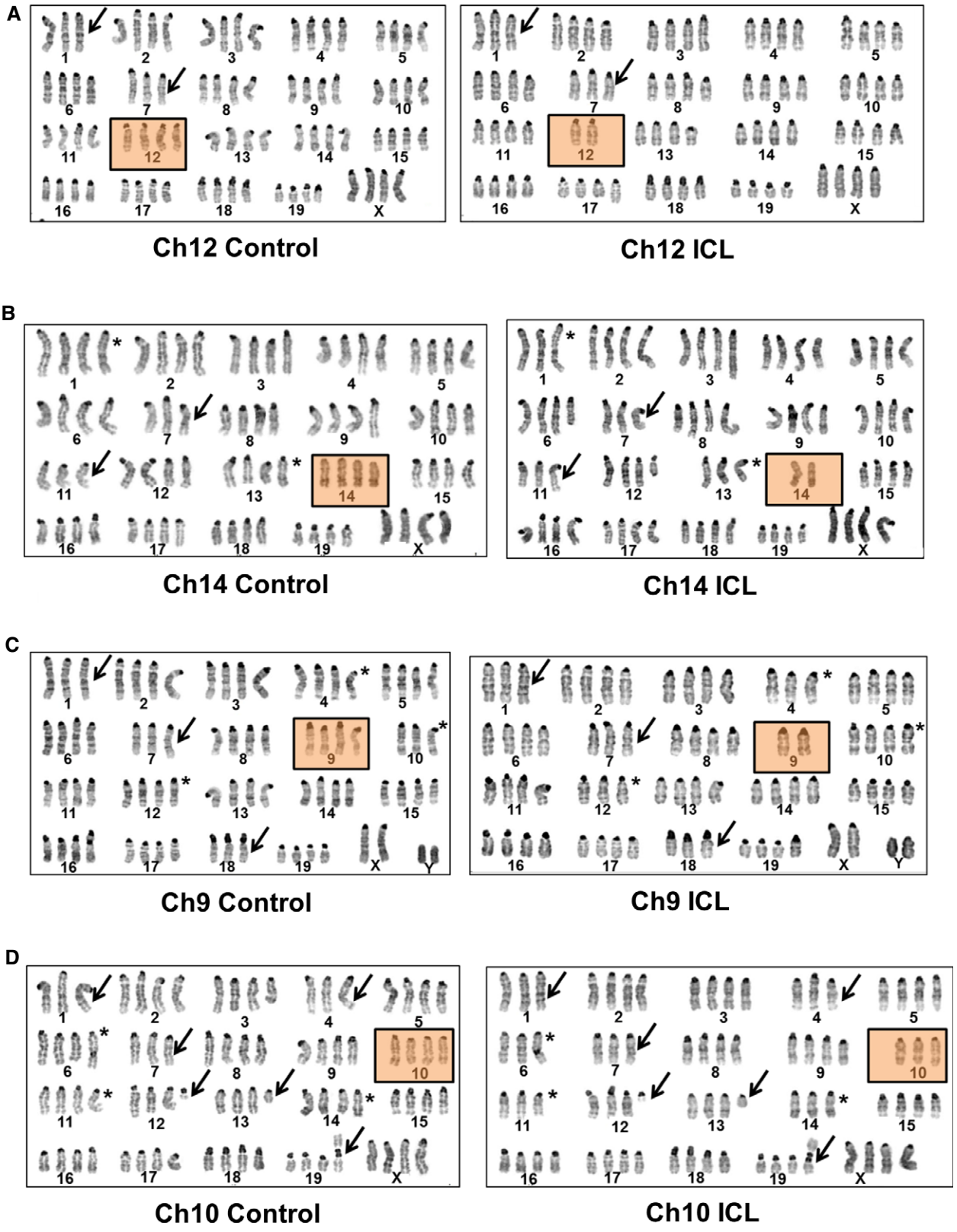


**Figure 3. Karyotypic characterization of the late passage ICL lines.**

A–D Representative karyotypes of late passage, large T antigen immortalized MEFs after exposure to Cre recombinase and serially sorted for control (hCD2 Plus) and ICL (hCD2 Minus) cells for chromosome lines (A) Ch12, (B) Ch14, (C) Ch9, and (D) Ch10. Boxed panels denote targeted chromosome loss; arrows and asterisks denote shared and unshared, non-targeted chromosomal copy number variations, respectively.

 

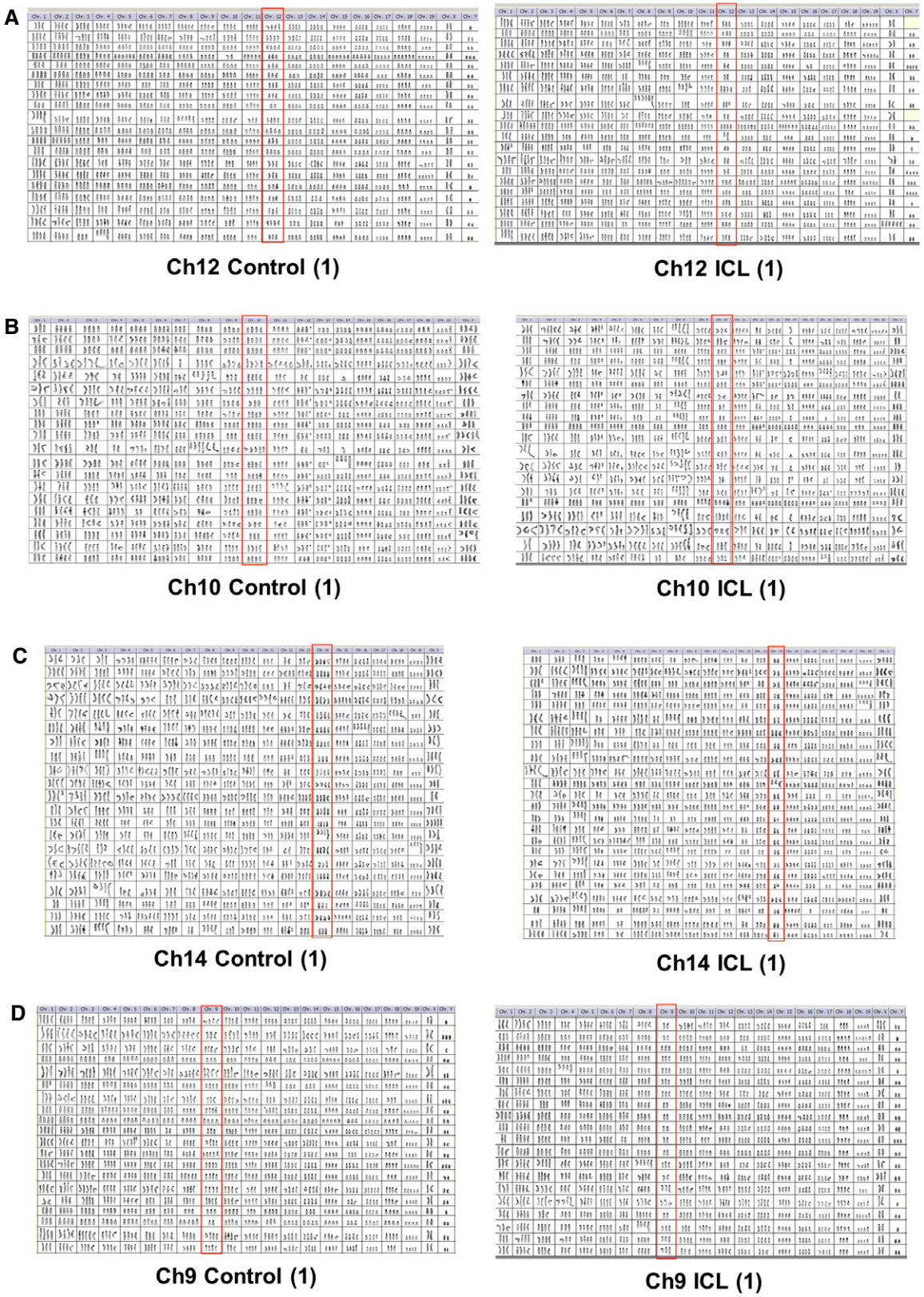


**Figure 4. Comprehensive karyotypic characterization of the late passage ICL lines.**

A–D Karyotypic analysis of later passage, control, and ICL of a replicate (#1) of Ch12 (A), Ch10 (B), Ch14 (C), and Ch9 (D) lines. All chromosomes are shown for 20 metaphases. Target chromosomes are boxed in red.

**Table 1. Chromosome copy number quantification from the karyotypes of late passage Ch9, 12, 10, and 14 MEFs.**

| | Ch9 control copy number | | Ch9 ICL copy number | | Ch12 control copy number | | Ch12 ICL copy number | | Ch10 control copy number | | Ch10 ICL copy number | | Ch14 control copy number | | Ch14 ICL copy number | |
|---|---|---|---|---|---|---|---|---|---|---|---|---|---|---|---|---|
| Ch | 4 | Non-4 | 4 | Non-4 | 4 | Non-4 | 4 | Non-4 | 4 | Non-4 | 4 | Non-4 | 4 | Non-4 | 4 | Non-4 |
| 1 | 7 | 13 | 2 | 18 | 12 | 8 | 7 | 13 | 0 | 20 | 0 | 20 | 4 | 17 | 3 | 21 |
| 2 | 19 | 1 | 20 | 0 | 19 | 1 | 19 | 1 | 18 | 2 | 18 | 2 | 18 | 3 | 16 | 8 |
| 3 | 17 | 3 | 18 | 2 | 19 | 1 | 17 | 3 | 17 | 3 | 8 | 12 | 17 | 4 | 15 | 9 |
| 4 | 17[b] | 3[b] | 2[b] | 18[b] | 19 | 1 | 15 | 5 | 2[b] | 18[b] | 12[b] | 8[b] | 17 | 4 | 10 | 14 |
| 5 | 19 | 1 | 19 | 1 | 19 | 1 | 17 | 3 | 19 | 1 | 16 | 4 | 13 | 8 | 15 | 9 |
| 6 | 16 | 4 | 20 | 0 | 18 | 2 | 16 | 4 | 19 | 1 | 17 | 3 | 13 | 8 | 18 | 6 |
| 7 | 0 | 20 | 0 | 20 | 1 | 19 | 1 | 19 | 0 | 20 | 0 | 20 | 3 | 18 | 0 | 24 |
| 8 | 15 | 5 | 18 | 2 | 19 | 1 | 18 | 2 | 17 | 3 | 7 | 13 | 18 | 3 | 16 | 8 |
| 9 | 13[a] | 7[a] | 0[a] | 20[a] | 16 | 4 | 16 | 4 | 17 | 3 | 15 | 5 | 16 | 5 | 15 | 9 |
| 10 | 18 | 2 | 18 | 2 | 17 | 3 | 19 | 1 | 16[a] | 4[a] | 0[a] | 20[a] | 20 | 1 | 18 | 6 |
| 11 | 17 | 3 | 19 | 1 | 18 | 2 | 15 | 5 | 17 | 3 | 12 | 8 | 2 | 19 | 1 | 23 |
| 12 | 14 | 6 | 10 | 10 | 8[a] | 12[a] | 0[a] | 20[a] | 17 | 3 | 7 | 13 | 11 | 10 | 6 | 18 |
| 13 | 17 | 3 | 16 | 4 | 19 | 1 | 20 | 0 | 15 | 5 | 9 | 11 | 5 | 16 | 1 | 23 |
| 14 | 16 | 4 | 18 | 2 | 16 | 4 | 19 | 1 | 16[b] | 4[b] | 5[b] | 15[b] | 17[a] | 4[a] | 0[a] | 24[a] |
| 15 | 18 | 2 | 20 | 0 | 19 | 1 | 19 | 1 | 19 | 1 | 17 | 3 | 17 | 4 | 17 | 7 |
| 16 | 16 | 4 | 20 | 0 | 18 | 2 | 19 | 1 | 15 | 5 | 7 | 13 | 20 | 1 | 21 | 3 |
| 17 | 18 | 2 | 19 | 1 | 20 | 0 | 20 | 0 | 14 | 6 | 6 | 14 | 21[b] | 0[b] | 16[b] | 8[b] |
| 18 | 16 | 4 | 12 | 8 | 17 | 3 | 18 | 2 | 18 | 2 | 13 | 7 | 18 | 3 | 16 | 8 |
| 19 | 17 | 3 | 15 | 5 | 19 | 1 | 16 | 4 | 17 | 3 | 17 | 3 | 18 | 3 | 19 | 5 |
| X | 20 | 0 | 18 | 2 | 18 | 2 | 13 | 7 | 15[b] | 5[b] | 4[b] | 16[b] | 10 | 11 | 13 | 11 |
| Y | 14 | 6 | 15 | 5 | | | | | | | | | | | | |

Repeat experiments were performed on ICL lines 9, 12, and 14, and no significant differences between ICL and control were observed in individual chromosomes in both replicates other than the targeted chromosome (data not shown). Since this Ch9 line was derived from a male embryo, the statistical tests for chromosomes X and Y were calculated for a copy number of 2 vs. non-2.

[a]Statistically significant loss of targeted chromosome loss in the respective ICL line, in relation to the corresponding control ($P < 0.05$, $n = 20$ metaphases for Ch9, 12, 10; $n = 21$ for Ch14 control and $n = 24$ for Ch14 ICL). Fisher exact test was used to determine statistical significance and a false discovery correction was applied to the *P*-values.

[b]Other significant chromosome number variations were not consistently observed in the same chromosome across all four lines ($P < 0.05$, $n = 20$ metaphases for Ch9, 10; $n = 21$ for Ch14 control and $n = 24$ for Ch14 ICL). Fisher exact test was used to determine statistical significance and a false discovery correction was applied to the *P*-values.

ICL chromosome lines (9, 10 and 14; Fig 5A). Collectively, these data indicate that later passage ICLs of mouse chromosomes 9, 10, and 14 result in a significant increase in the *in vivo* tumorigenic potential.

As seen with the early passage cells, the later passage growth rate in cell culture was either the same or lower in the ICLs vs. controls. Three out of our four ICL lines (Ch10, 12, 14) grew significantly slower *in vitro* relative to their controls, suggesting reduced cellular fitness (Fig 6A and Appendix Fig S3A). The fourth ICL line missing Ch9 had no significant change in growth rate (Appendix Fig S3A). ICL cells also formed fewer colonies when plated at very low seeding, further implying an *in vitro* growth defect (Fig 6B). Thus, expansion of the ICL lines in culture maintained or enhanced the tumorigenic potential of the lines, which had initially lost a single chromosome and similarly did not affect the relative growth rates in cell culture. All ICL lines showed a significant growth advantage over the controls under anchorage-independent conditions (Fig 6C), a property consistent with their enhanced tumorigenic potential. When the ICL lines were explanted from the tumors, they did not retain the proliferative advantage (seen *in vivo*) highlighting that the growth advantage is manifested only under conditions requiring anchorage independence (Appendix Fig S3B).

In order to determine whether metabolic changes characteristic of certain tumors and trisomic MEFs were also present in our ICL cells, we performed metabolite analysis on the conditioned media from these cells (Williams *et al*, 2008). Ch14 ICL cells had increased levels of lactate production and glucose consumption in comparison with the Ch14 controls (Fig 6D). These altered metabolic phenotypes were not manifested in Ch9, Ch10, and Ch12 ICL cells, suggesting that metabolic changes are likely chromosome-specific effects.

Taken together, given that the tumor phenotypes of at least two ICL lines (9 and 14) were observed prior to the accrual of any non-targeted chromosomal anomalies, argues strongly that these

 

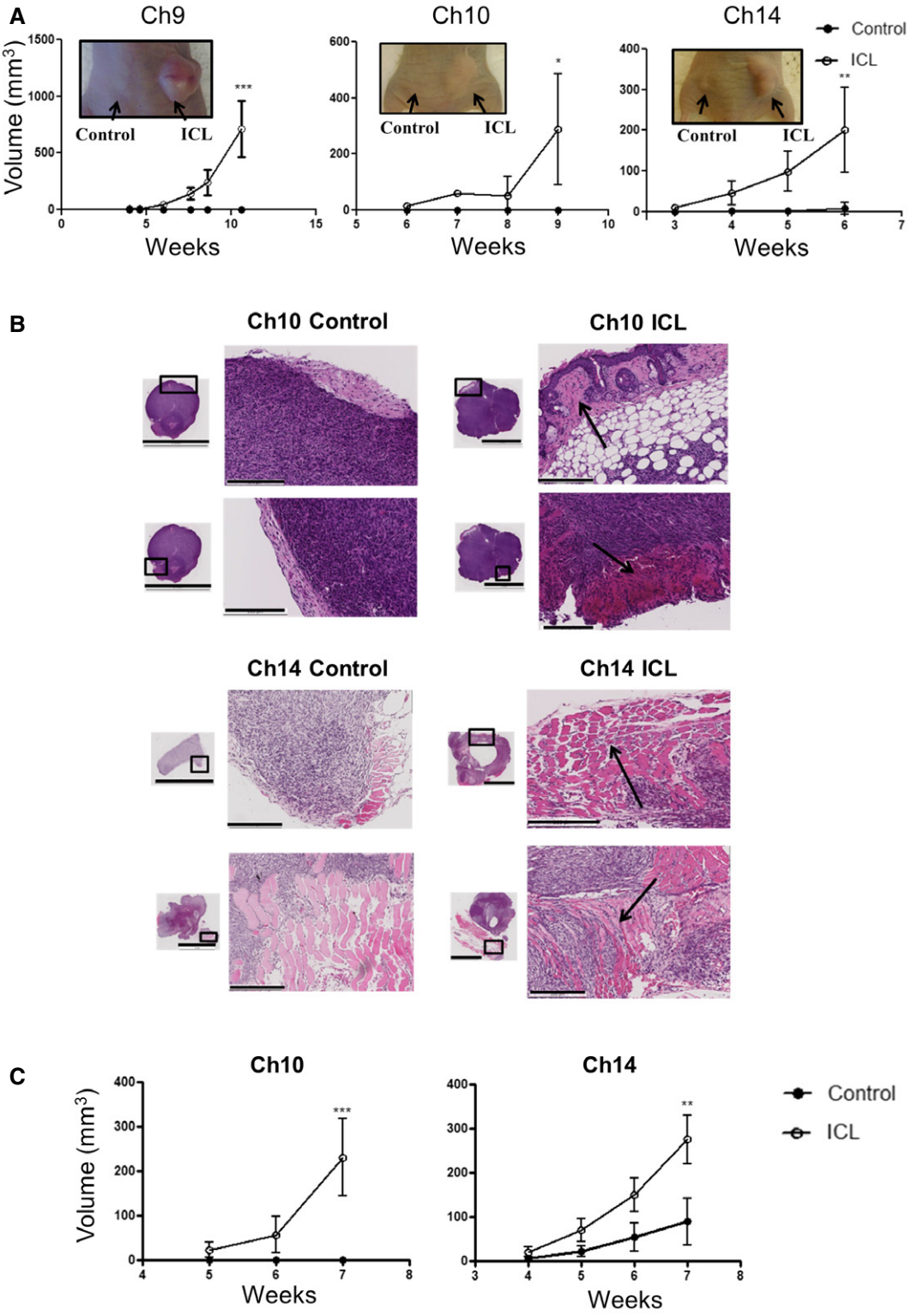


**Figure 5. Tumorigenic potential of late passage aneuploid cells.**

A Tumor growth curve after later passage ICL cells were injected into flanks of athymic nude mice ($n$ = 5 per group and error bars denote SD, ***$P < 0.0005$ for Ch9, *$P < 0.05$ for Ch10 and **$P < 0.005$ for Ch14). Two-tailed unpaired $t$-test was used to determine statistical significance.

B Tumor sections were stained with H&E to assess tumor histology (scale bars denote 5 mm for the inset and 200 μm for the zoomed image). Arrows in the ICL tumors sections indicate regions where tumors have invaded into the adjacent tissue.

C Tumor growth curve after later passage ICL cells were injected into flanks of NOD/SCID mice ($n$ = 5 per group and error bars denote SD, ***$P < 0.0005$ for Ch10 and **$P < 0.005$ for Ch14). Two-tailed unpaired $t$-test was used to determine statistical significance.

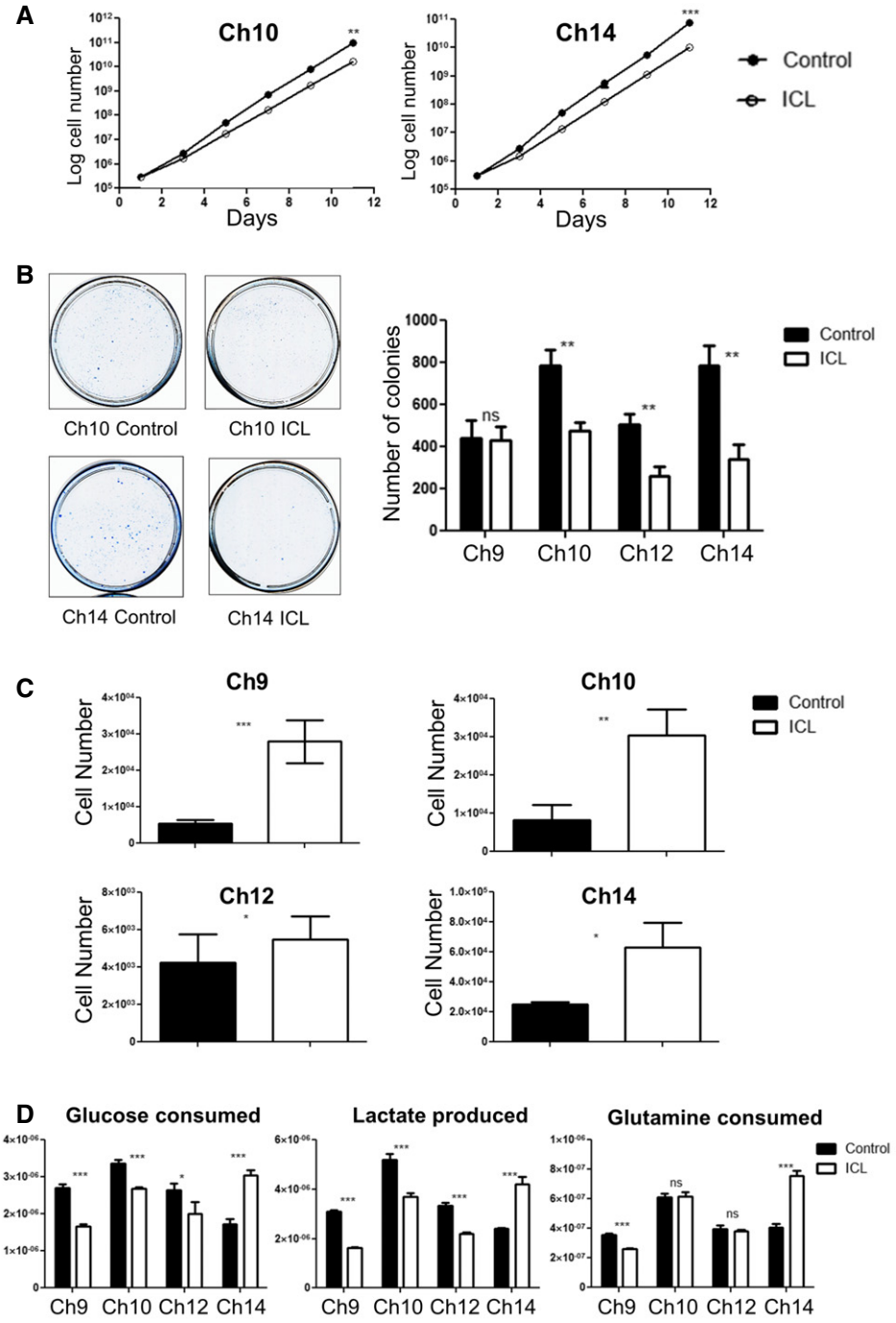


**Figure 6.** ***In vitro*** **characterization of later passage ICL MEFs.**

A Growth curve of the later passage ICL lines Ch10 and Ch14 under adherent *in vitro* culture conditions ($n$ = 3 for each data set and error bars denote SD, $^{**}P < 0.005$ for Ch10 and $^{***}P < 0.0001$ for Ch14). See also Appendix Fig S3A. Two-tailed unpaired $t$-test was used to determine statistical significance.

B Colony formation in ICL and control MEFs. 5,000 cells were seeded in 10-cm plates and stained with methylene blue after 3 days. Representative colony formation images in Ch10 and Ch14 are shown (left) and quantification of colonies formed (right) in the 4 ICL lines ($n$ = 3 for each data set and error bars denote SD, $^{**}P < 0.005$ for Ch10, Ch12, and Ch14 and ns for Ch9). Two-tailed unpaired $t$-test was used to determine statistical significance.

C Quantification of growth in ultra-low adherent, sphere-forming conditions for the four ICL lines ($n$ = 3 for Ch10 and Ch14, $n$ = 6 for Ch9 and Ch12 and error bars denote SD, $^{***}P < 0.0001$ for Ch9, $^{**}P < 0.001$ for Ch10 and $^{*}P < 0.05$ for Ch12 and Ch14). Two-tailed unpaired $t$-test was used to determine statistical significance.

D Analysis of metabolites (glucose consumed, lactate produced and glutamine consumed) for the ICL lines. Spent media was analyzed after each ICL, and control line was grown in culture for 3 days. Media in identical culture conditions, but with no plated cells, was used as a baseline for all samples ($n$ = 3 for each data set and error bars denote SD; Glucose consumed: $^{***}P < 0.0005$ for Ch9 and Ch14, $^{***}P = 0.0005$ for Ch10 and $^{*}P < 0.05$ for Ch12; Lactate produced: $^{***}P < 0.0005$ for Ch9 and Ch12, $^{***}P = 0.0008$ for Ch10, and $^{***}P = 0.0005$ for Ch14; Glutamine consumed: $^{***}P < 0.0005$ for Ch9 and Ch14). Two-tailed unpaired $t$-test was used to determine statistical significance.

 

targeted chromosomal aberrations were the driving event in the acquisition of tumorigenicity. We cannot rule out the possibility that Ch10 ICL, which acquired tumor potential only after longer passaging, had suffered other events that facilitated their transformation. We suspect that the initial distal loss of Chr10 must at least be contributing to the tumor phenotype since, in the four different Ch10 lines examined, only the ICLs (and never the control cell lines), after extensive passaging, ever acquire tumorigenic potential.

#### Effects of tetraploidy and chromosome identity on tumorigenicity

Induced chromosome loss of Ch12 consistently did not produce tumors, arguing against the possibility that any breakage and rejoining events *per se* that take place during the process of chromosome loss transforms immortalized MEFs. Also, the basal aneuploidy arising from the tetraploidization and/or p53/pRb attenuation observed in the parental control lines was not sufficient to form tumors in the mice, suggesting a critical role for the targeted chromosome loss in tumorigenesis. We note that tetraploidization of our ICL lines may be required to manifest the tumorigenic potential upon chromosome loss. MEFs immortalized using short hairpins against p19 are known to be diploid in early passages (Kamijo *et al*, 1997; Zindy *et al*, 1997; Randle *et al*, 2001). p19 immortalized diploid MEFs with targeted chromosome losses (Ch10 and 14) did not produce tumors (Appendix Fig S4). In addition, to test the effects of chromosome loss in an independent diploid model *in vivo*, a knock-in allele of Id1 driving tamoxifen-inducible Cre recombinase was employed in the Ch10 and Ch14 iLoxP mice (Nam & Benezra, 2009). Id1 is expressed in long-term repopulating hematopoietic stem cells (Jankovic *et al*, 2007) and other stem cell populations (Nam & Benezra, 2009). While ~50% of the blood cells in these mice exhibited hCD2 marker loss at 30 days post-Cre induction, at a later time point (80 days), this number dropped to 17%, indicating that the monoploid cells have a proliferative disadvantage in comparison with the diploid population (Fig 7A). This suggests that the effects of inducing chromosome loss can have different effects depending on the original ploidy and the tissue type where aneuploidy is induced. It is noteworthy that in the vast majority of human tumors with numerical chromosome losses, the modal chromosome number is > 2N (both on an individual chromosome basis and for any chromosome in general; Fig 7B and C), implying that the tetraploid state is a clinically relevant background to assess the contribution of chromosome losses to tumorigenesis.

The variation in tumorigenic properties and tumor latency between the ICL lines suggests that there may be chromosome-specific effects with regard to tumorigenesis. Highlighting this, Davoli *et al* (2013) used a computational method to assign "CHROM" scores to human chromosomes based on the mutational signatures of 300 highest ranked tumor suppressor genes (TSGs) and 250 oncogenes (OGs) and observed that in human tumors, chromosomes with a higher CHROM score (high density of top-ranked TSGs) were lost more frequently. We mapped these human TSGs and OGs onto mouse chromosomes and observed that while tumor suppressor genes from these ranked lists were present on Ch14 (high density of top-ranked TSGs) and Ch9 (moderate density), Ch10 and 12 were largely devoid of highly ranked TSGs (Table 2). While higher density of potent TSGs for Ch9 and Ch14 would be expected to be associated with increased tumorigenic potential upon chromosome loss, a lack of highly ranked TSGs by itself did not result in failure to form tumors, as demonstrated in the Ch10 ICL cells, which readily formed tumors. Thus, both general chromosome loss effects, as well as chromosome-specific effects, likely contribute to tumorigenic potential in this model system.

#### ICL induced genomic instability and DNA damage

In an attempt to understand the mechanism by which the ICL lines became inherently better suited for anchorage-independent growth (and by inference tumor growth), we analyzed their ability to undergo an epithelial-to-mesenchymal transition (EMT) more rapidly than parental controls or activate pro-proliferative pathways and/or autophagy, as these are common mechanisms by which cells attain anchorage independence (Guadamillas *et al*, 2011). We found no clear changes in these measures suggesting that other mechanisms are driving the observed phenotypes (data not shown). Aneuploidy has been shown to potentially cause a mutator phenotype that further induces more genomic instability, which could facilitate adaptation to the stresses of anchorage-independent growth. In haploid yeast strains, for example, addition of an extra chromosome caused genomic instability phenotypes like chromosome mis-segregation errors and increased mutation rate (Sheltzer *et al*, 2011). In *Saccharomyces cerevisiae*, aneuploidy caused by Hsp90 inhibition enabled yeast strains to adapt well to other unrelated stress conditions by inducing karyotypic diversity (Chen *et al*, 2012). Additionally, trisomic MEFs with certain oncogenic activations acquired new karyotypic changes at later passages that provided better adaptive fitness to these cells (Sheltzer *et al*, 2017).

For these reasons, we sought to determine whether the induced aneuploid cells had evidence of further genomic instability beyond changes in the targeted chromosomes. Karyotyping analysis revealed increased chromosome instability in all later passage ICL lines *in vitro,* demonstrated by increased average chromosome loss per metaphase relative to the control counterparts (6.2 vs. 4.2 for Ch9, $P < 0.005$; 12.3 vs. 5.7 for Ch10, $P < 0.0001$; 4.8 vs. 2.9 for Ch12, $P < 0.05$ and 11.8 vs. 6.6 for Ch14, $P < 0.0001$), average structural rearrangements per metaphase (5.3 vs. 1.5 for Ch9, $P < 0.0001$; 14.2 vs. 8.5 for Ch10, $P < 0.0001$; 2 vs. 1.1 for Ch12, $P < 0.05$ and 11 vs. 6.7 for Ch14, $P < 0.05$) and percentage of metaphases with marker chromosomes (chromosome fragments; 90 vs. 75 for Ch9, ns; 80 vs. 20 for Ch10, $P < 0.0005$ and 35 vs. 15 for Ch12, ns; Fig 8A). Also, compared to the controls, we observed an increase in basal γH2AX foci per nuclei (a read-out of DNA double strand breaks) in ICL cells (124 vs. 92 in Ch9, $P < 0.0001$; 102 vs. 53 in Ch10, $P < 0.0001$; 97 vs. 67 in Ch12, $P < 0.0001$; 78 vs. 63 in Ch14, $P < 0.05$; Fig 8B). The increase in γH2AX foci in the ICL cells was also observed when the cells were grown in the low adherence sphere-forming conditions (73 vs. 47 in Ch10; $P < 0.0001$ and 75 vs. 47 in Ch14, $P < 0.0001$; Appendix Fig S5A). Surprisingly, we noticed that the ICL lines exhibited a modest yet significant increase in the percentage of cleaved caspase-positive cells, an apoptosis marker, despite not displaying signs of cell death (13.1 vs. 0.8% in Ch9, $P < 0.0001$; 2.0 vs. 1.0% Ch10, $P < 0.05$; 1.3 vs. 0.9% in Ch12, $P < 0.05$ and 0.7 vs. 0.2% in Ch14, $P < 0.0005$; Appendix Fig S5B). This may also contribute to the enhanced mutator phenotype.

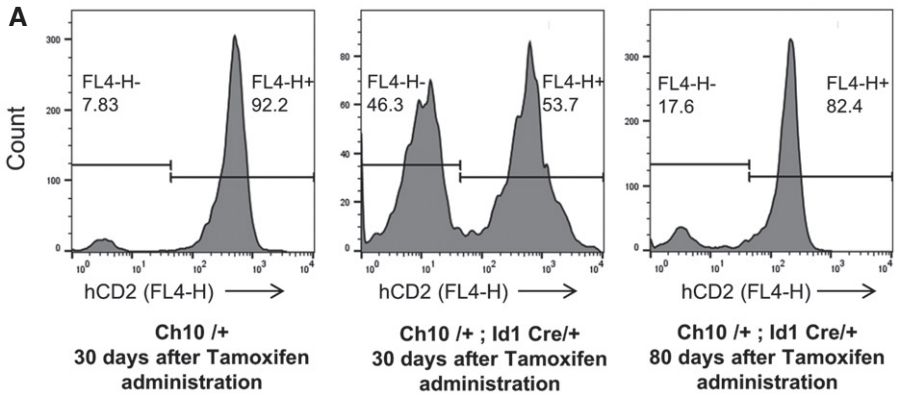


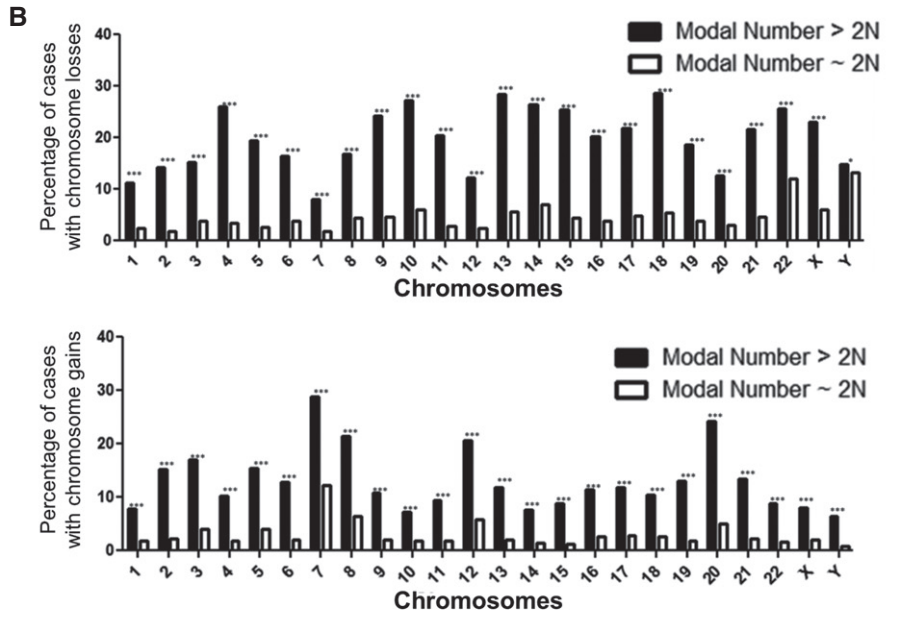


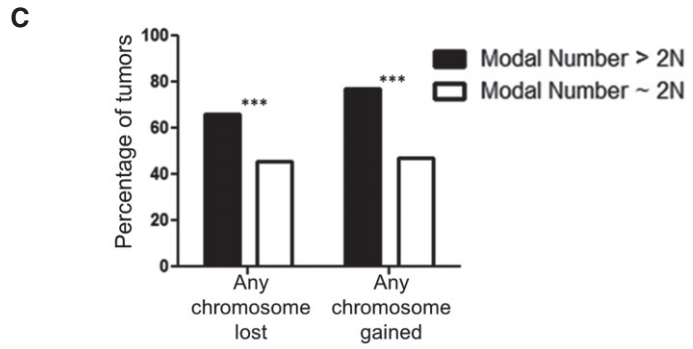


**Figure 7. Effects of ploidy on the tumorigenic potential of ICL cells.**

A Flow cytometry analysis of tail blood from Ch10/+ (control) at 30 days post-tamoxifen administration, Ch10/+; Id1 Cre/+ at 30 days post-tamoxifen administration, and Ch10/+; Id1Cre/+ at 80 days post-tamoxifen administration.

B Analysis from the Mitelman database for the fraction of human solid tumors that have lost (top) or gained (bottom) individual chromosomes that have modal chromosome number > 2N or ~2N ($n$ = 3,459 cases for modal number > 2N and $n$ = 12,464 cases for modal number ~2N, top: ***$P < 0.0001$ for chromosomes 1–22, X and *$P < 0.05$ for chromosome Y; bottom: ***$P < 0.0001$ for all chromosomes). Two-tailed two-sample $t$-test to compare sample means was used to determine statistical significance.

C Analysis from the Mitelman database for the fraction of human solid tumors that have lost or gained any chromosome that have modal chromosome number > 2N or ~2N ($n$ = 3,459 cases for modal number > 2N and $n$ = 12,464 cases for modal number ~2N, ***$P < 0.0001$ for both modal number > 2N and ~2N). Two-tailed two-sample $t$-test to compare sample means was used to determine statistical significance.

 

**Table 2. Ranked list of the 300 tumor suppressor genes on mouse chromosomes 9, 10, 12, and 14 after being mapped from the human chromosomes, preserving their original CHROM rank. Loss of smaller ranked TSGs contributed most to tumorigenesis in the human tumors.**

| Gene name | Mouse chromosome | Potency rank |
|---|---|---|
| DNMT3A | 12 | 60 |
| ZFP36L1 | 12 | 74 |
| FANCM | 12 | 116 |
| FOXA1 | 12 | 118 |
| TRAF3 | 12 | 128 |
| ARHGAP5 | 12 | 153 |
| ASXL2 | 12 | 158 |
| NEK9 | 12 | 183 |
| BTBD7 | 12 | 219 |
| DAAM1 | 12 | 236 |
| MOAP1 | 12 | 244 |
| YLPM1 | 12 | 274 |
| PBRM1 | 14 | 6 |
| Rb1 | 14 | 7 |
| BAP1 | 14 | 33 |
| Zc3h13 | 14 | 36 |
| AJUBA | 14 | 77 |
| CHD8 | 14 | 87 |
| Sox21 | 14 | 131 |
| Dach1 | 14 | 143 |
| DENND6A | 14 | 154 |
| Rbm26 | 14 | 164 |
| SPCS1 | 14 | 208 |
| NFATC4 | 14 | 225 |
| TTC18 | 14 | 227 |
| PPP3CC | 14 | 261 |
| Kbtbd7 | 14 | 263 |
| SETD2 | 9 | 15 |
| ATM | 9 | 25 |
| TGFBR2 | 9 | 47 |
| SMARCA4 | 9 | 51 |
| USP28 | 9 | 65 |
| KEAP1 | 9 | 82 |
| MYO6 | 9 | 91 |
| TCF12 | 9 | 101 |
| KMT2A | 9 | 102 |
| SIN3A | 9 | 130 |
| HERC1 | 9 | 142 |
| TMEM30A | 9 | 212 |
| RNF111 | 9 | 250 |
| DOPEY1 | 9 | 252 |
| ATR | 9 | 275 |
| SIK3 | 9 | 278 |
| STK11 | 10 | 38 |
| SMARCB1 | 10 | 75 |
| MBD6 | 10 | 93 |
| CCAR1 | 10 | 97 |
| JMJD1C | 10 | 114 |
| RUFY2 | 10 | 155 |
| MED23 | 10 | 157 |
| HDAC2 | 10 | 165 |
| STX7 | 10 | 167 |
| ATG5 | 10 | 195 |
| PTPRK | 10 | 203 |
| TMPO | 10 | 210 |
| GNPTAB | 10 | 221 |
| CCDC38 | 10 | 288 |

Similarly, tumors derived from ICL lines showed increased numbers of γH2AX-positive cells in comparison with the controls (4.4 vs. 1.8% in Ch10, $P < 0.0001$ and 3.7 vs. 2.4% in Ch14, $P < 0.05$; Fig 8C) and a generally increased chromosomal instability phenotype as evidenced by the increase in the average chromosome loss per metaphase (20.8 vs. 9.4 for Ch10, $P < 0.0001$; 13.5 vs. 12.4 for Ch14, ns), average structural rearrangements per metaphase (14.4 vs. 11.2 for Ch10, $P < 0.05$; 14.6 vs. 11.3 for Ch14, $P < 0.05$) and percentage of metaphases with marker chromosomes (65 vs. 24% for Ch10, $P < 0.05$; 100 vs. 100% for Ch14, ns; Fig EV4). Together, these data indicate that the later passage ICL lines are associated with high levels of chromosomal instability and DNA damage and this mutator phenotype could potentially allow the ICL cells to sample more karyotypic space. We recognize that this mutator phenotype is not sufficient for transformation, as Ch12 ICL cells did not form tumors despite having elevated DNA damage. Thus, while the mutator phenotype may be required to enable the ICL cells to adapt well to stress conditions (such as enhanced growth in substratum-free conditions and in the subcutaneous space of mice), there may be other mechanisms intrinsic to chromosome loss that are required for tumorigenesis.

## Discussion

In this study, we have successfully adapted the iLoxP inverted recombination system to generate an aneuploidy model, inducing targeted chromosome losses and generating dicentric fragments, in the context of a tetraploid state, without perturbing the expression of a specific protein. Variations of this method have also been used previously to introduce various genomic aberrations in mice (Lewandoski & Martin, 1997; Gregoire & Kmita, 2008; Zhu *et al*, 2010). We found that ICL of mouse chromosomes, while not providing a substantial growth advantage under normal *in vitro* conditions, facilitated growth under the stressful conditions of anchorage-independent growth and *in vivo* tumor formation. The parental

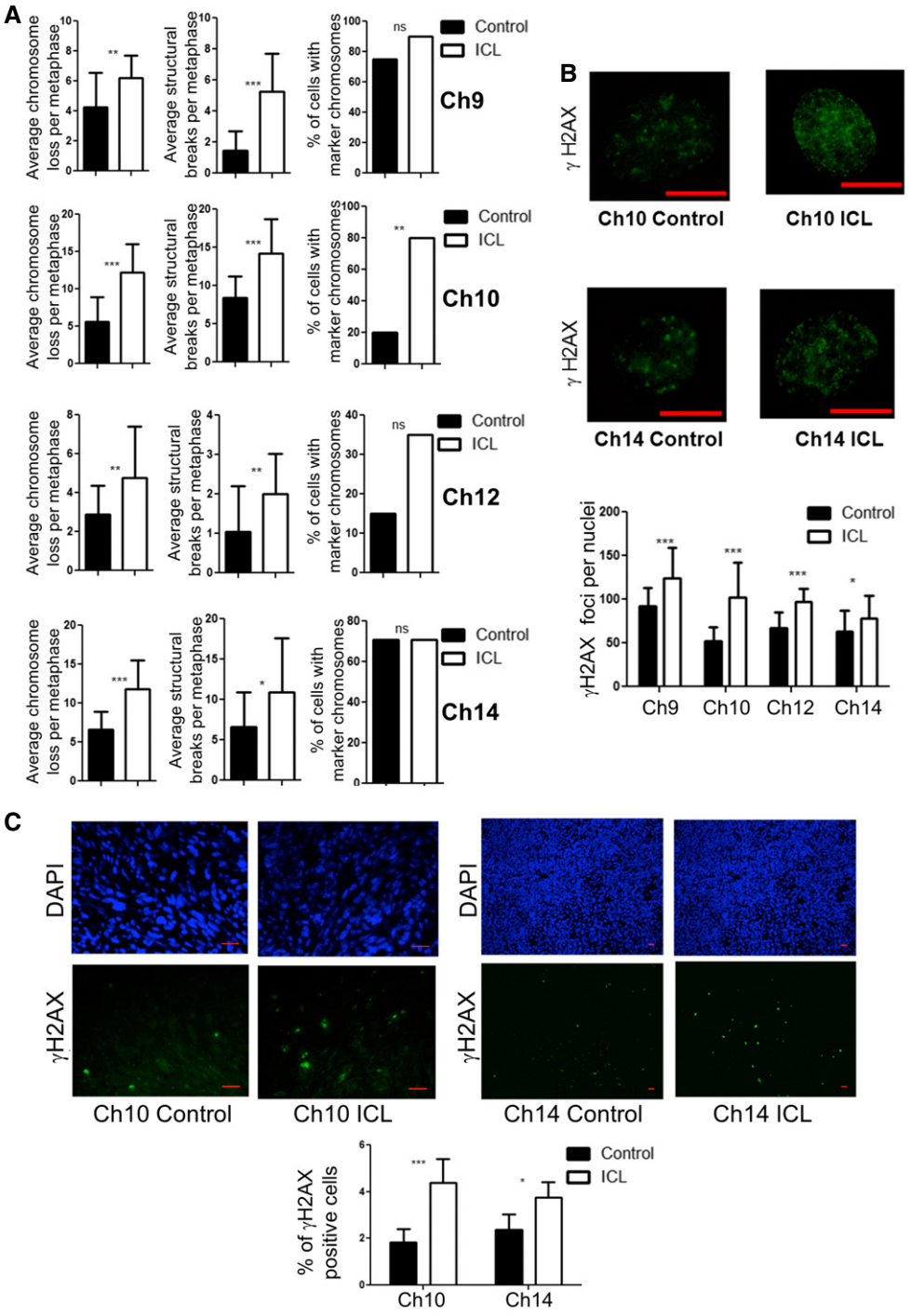


**Figure 8. Increased chromosomal instability and DNA damage in ICL *in vitro* lines and tumors.**

A Chromosomal instability readouts, of later passage lines, assessed by average chromosomes loss per metaphase, average number of structural rearrangements per metaphase and percentage of metaphases with marker chromosomes ($n$ = 20 for each data set and error bars denote SD, average chromosome loss: $^{**}P < 0.005$ for Ch9, $^{***}P < 0.0001$ for Ch10 and Ch14, and $^{**}P < 0.05$ for Ch12; average structural rearrangements: $^{***}P < 0.0001$ for Ch9 and Ch10, $^{**}P < 0.05$ for Ch12, and $^{*}P < 0.05$ for Ch14; percentage of metaphases with marker chromosomes: $^{**}P < 0.0005$ for Ch10). Two-tailed unpaired t-test was used to determine statistical significance for average chromosome loss and structural breaks. Two-tailed $Z$-test was used to determine statistical significance for the percentage of cells with marker chromosomes.

B Determination of number of γH2AX foci in ICL and control nuclei and quantification (scale bars denote 10 μm, $^{***}P < 0.0001$ for Ch9, Ch10, and Ch12, $^{*}P < 0.05$ for Ch14; $n$ = 25 for each data set, and error bars denote SD). See also Appendix Fig S5A and B. Two-tailed unpaired $t$-test was used to determine statistical significance.

C Number of γH2AX-positive cells in formalin fixed ICL and control tumor sections by immunofluorescence staining and quantification (Scale bars denote 20 μm, $n = 8$ fields for Ch10 and 5 fields for Ch14 with at least 200 cells in each field, $^{***}P < 0.0001$ for Ch10 and $^{*}P < 0.05$ for Ch14). Two-tailed $Z$-test was used to determine statistical significance.

 

controls in later passages, which exhibited a minor degree of aneuploidy independent of the targeted chromosome loss, showed no or reduced growth in immunocompromised mice compared to matched ICL lines. This observation was consistent across multiple separate ICL lines for a given chromosome, as well as across multiple chromosomes. Further, in early passage MEFs, the only pronounced copy number change was in the targeted chromosomes, and in two out of the four chromosome lines tested, this targeted change alone was sufficient to drive tumorigenesis. Taken together, these results demonstrate that the initial loss of the targeted chromosome along with the genomic instability associated with the BFB cycles of the dicentric fragments (see later section for the discussion on BFB-mediated genomic rearrangements) is critical for these tumor phenotypes. We note that recent data suggest that aneuploid cells may thrive in human tumors due to escape from immune surveillance (Davoli *et al*, 2017). Our data in immunocompromised mouse models argue for an additional immune-independent growth advantage of aneuploid cells.

While there are deviations from the baseline copy number of 4 in a few chromosomes in the later passage control lines, we speculate that the reasons that these aberrations are not sufficient to initiate *in vivo* tumors are (i) these baseline changes in the control lines are not as penetrant as the targeted losses in the ICL lines in the population, and therefore, the ensuing instability is below the threshold to similarly accelerate tumorigenesis and/or, (ii) the reduction to copy number of 2 is necessary to manifest the tumor phenotype (which is observed only in the ICL cells). We also observed that the initial copy number variation in the targeted chromosome, irrespective of the identity of the targeted chromosome, induced a significant increase in chromosomal instability, DNA damage, and secondary chromosome losses. This feature could enable the ICL cells to sample more genomic permutations and enable them to thrive under stressful, substratum-free conditions. Thus, in addition to maintaining the loss of the targeted chromosome, the ICL cells accumulated other chromosomal changes more rapidly than the controls. Other models of whole chromosome aneuploidy also generate a mutator phenotype, causing further chromosomal instability and DNA damage (Janssen *et al*, 2011; Sheltzer *et al*, 2011; Crasta *et al*, 2012). In addition, DNA damage has been shown to increase chromosome instability through the stabilization of kinetochore–microtubule interactions (Bakhoum *et al*, 2014) thereby forming a possible feed forward loop of chromosomal instability. Whether enhanced chromosome mis-segregation observed in the ICL lines is a cause or consequence of enhanced DNA damage and how this cycle is started by the initiating chromosome loss event will require further study.

After the inverted Cre recombination, the dicentric fragments, which undergo BFB cycles, could invade and integrate randomly into other regions of the genome (instead of being lost) thereby promoting genomic instability and tumorigenesis. BFB cycles of dicentric fragments are a common cause of chromosome loss in cancer cells, and such events have been shown to induce genomic redistribution, genomic instability, and tumor heterogeneity in a variety of tumor types (Artandi *et al*, 2000; Gisselsson *et al*, 2000; Selvarajah *et al*, 2006). Dicentric fragments can also result in chromothripsis, a catastrophic chromosome shattering, and reorganization phenomenon. In this model, instead of being broken, the dicentrics result in the formation of chromatin bridges, leading to nuclear envelope rupture and DNA repair, and eventually to structurally reorganized chromosomes (Maciejowski *et al*, 2015). Mis-segregating chromosomes (that lead to whole chromosome losses in the daughter cells) have also been shown to trigger gross genomic redistributions. The mis-segregating chromosomes induce micronuclei formation, where they are pulverized and then integrated back into the genome (Crasta *et al*, 2012). Mis-segregating chromosomes also produce structural chromosomal changes by being trapped and damaged in the cleavage furrow during cytokinesis, leading to DNA breaks and unbalanced translocations (Janssen *et al*, 2011). Thus, two processes, pure chromosome loss events and structural genomic rearrangements, are intimately connected. Though we cannot distinguish between the contributions of these two processes to transformation, our model to induce chromosome loss via the formation of dicentrics nonetheless attempts to faithfully mimic the actual evolution of cancer cells.

We note that the tumorigenic potential of the ICL lines is manifested only in a tetraploid background. This benefit of chromosome copy number reductions from a tetraploid genome is consistent with previous data from other groups. Tetraploid mouse cells have been shown to lose chromosomes when they form tumors in mice, suggesting that tetraploidy may be a state where chromosome loss is better tolerated or even beneficial (Davoli & de Lange, 2012). $p53^{-/-}$ tetraploid mouse mammary epithelial cells were more prone to whole chromosome aneuploidies than their diploid counterparts and the tetraploidization promoted tumor formation of these cells in nude mice (Fujiwara *et al*, 2005). Also, it has been shown, using *in silico* analyses, that a near triploid state endows the maximum fitness to the adaptation of the cancer cells (Laughney *et al*, 2015). Importantly, in this study, the tetraploid state (rather than the diploid state) has a shorter barrier to reach the near triploid state. In addition, Carter *et al*, using a computational method, showed that whole genome doublings are common occurrences in human tumors and that the evolved karyotype of these tumors is a result of losing chromosomes after the initial doubling (as opposed to sequential gaining of chromosomes on a diploid background; Carter *et al*, 2012). Thus, these studies highlight the importance of passing through a tetraploid state followed by chromosome losses in tumorigenesis.

In summary, our ICL model demonstrates that individual chromosome loss events, along with BFB-mediated chromosomal instability, in a tetraploid background can be a potent driver of tumorigenesis in mouse cells and provides a new platform to further our understanding of the consequences of whole chromosome loss events in cancer.

## Materials and Methods

### Mouse embryonic fibroblasts FACS sorting

Primary mouse embryonic fibroblasts from Ch9, 10, 12, and 14 mouse lines were isolated from mice at day 13.5 post-coitum (p.c.) and were immortalized by transfecting with SV40 large T antigen. Immediately after the primary MEFs were isolated and cultured from the embryos, they were transfected with a plasmid containing SV40 large T antigen. Once the transfected MEFs attained 90% confluence, they were split from one 6 well entirely

into a 10-cm dish. After they attained 90% confluence in the 10-cm dish, they were split at a ratio of 1:10 into another 10-cm dish (passage dilution factor 10). This procedure was serially repeated till the passage dilution factor becomes $10^6$, by when the primary MEFs that have successfully been transfected with the SV40 large T antigen, were immortalized, while the primary cells were out competed (as they senesced). Two independent biological replicates (completely separate MEF lines followed by independent immortalization and FACS sorting procedures) were used for the Ch12 ICL lines, and similarly, three biological replicates were used for Ch10, Ch14, and Ch9 lines. Representative results are provided in the manuscript from these replicates. Recombination between the iLoxP sites was induced in Ch10 and Ch14 immortalized MEFs, which expressed a ubiquitous tamoxifen-responsive CreER (RNA PolII CreER, *RERT*), by treating with 1 μM 4-hydroxy tamoxifen (4OHT) for 14 days. Recombination was induced in Ch9 and Ch12 immortalized MEFs by transducing with an adenovirus expressing Cre recombinase for 18 h. We have also performed similar experiments using Adeno-Cre on Ch10 and Ch14 MEFs and found consistent results as previously generated using 4OHT. "Early passage MEFs" denoted 2 weeks postsort and "Late passage" denoted 4 weeks postsort. Recombined MEFs were stained with an hCD2 antibody (BD Pharmingen) and flow sorted to obtain hCD2 Plus (control) and hCD2 Minus (ICL) populations.

#### Growth rates, seeding efficiency, and metabolite analysis

For determining the growth rates, 300,000 cells were plated in triplicate in 60-mm tissue culture dishes (or 50,000 cells in each well of six-well plates). After every 2 days, cells were trypsinized, counted, and re-plated at the starting density. For seeding efficiency measurements, 5,000 cells were plated in 100-mm culture dishes. After 3 days, cells were stained with 0.05% methylene blue and the colonies were counted. For metabolite analysis, cells were plated as described for growth curves. After 3 days, growth media was collected, spun down to remove debris and residual cells, and analyzed using an YSI 7100 MBS Mutliparameter Bioanalytical System to obtain metabolite concentrations for glucose, lactate, and glutamine. Cell culture media from plates exposed to identical culture conditions but without plated cells was used as the baseline. Two-tailed unpaired *t*-test was used to determine statistical significance.

#### Growth in immunocompromised mice

Induced chromosome loss cells and their respective controls were injected into the flanks of athymic nude mice at a cell density of 250,000 in 200 μl phosphate buffer for later passage Ch10, Ch14 cells; 1,000,000 in 200 μl phosphate buffer for later passage Ch9, Ch12 cells; 5,000,000 in 200 μl phosphate buffer for early passage Ch14 cells; and 15,000,000 in 200 μl phosphate buffer for early passage Ch9 cells. These mice were monitored for tumor formation, and tumor dimensions were measured weekly. The tumor volume was calculated using the formula $\text{Volume} = 0.5 \times \text{Length} \times (\text{width})^2$. Two-tailed unpaired *t*-test was used to determine statistical significance. All the immunocompromised mice were ordered from Taconic Biosciences. Housing regulations and experimentation on the mice were approved by the MSKCC Institutional Animal Care and Use Committee (IACUC) and Research Animal Resource Center (RARC).

#### Karyotypes and Shallow whole-genome sequencing

For metaphase spreads, one million cells were plated in a 10-cm dish and after 24 h treated with 0.2 μM colcemid for 4 h. Cells were trypsinized, incubated in 75 mM KCl, and fixed with 75% methanol: 25% acetic acid mixture for 5 min. After two additional washes with fixative, cells were dropped from a height of about 2 inches on pre-chilled glass slides, which were held over a water bath. Slides were allowed to dry overnight and stained with 0.02% Giemsa and submitted for karyotype analysis. Images were analyzed using Applied Spectral Imaging. Fisher exact test was performed to calculate statistical significance of chromosome number variation between the controls and the ICL metaphases, and a false discovery correction was applied to the *P*-values. For the chromosomal instability readouts, two-tailed unpaired *t*-test was used to determine statistical significance for average chromosome loss and structural breaks per metaphase. A two-tailed *Z*-test was used to determine statistical significance for the percentage of cells with marker chromosomes. Shallow WGS was carried out at the Integrated Genome Operations core facility at MSKCC. 50 ng of purified DNA from each control and ICL line was sequenced on Illumina HiSeq2000 (10 million reads per sample with 100mer paired-end sequencing). The sequencing results were aligned to mouse mm9 genome, and copy number changes were estimated in 300 kb bins.

#### Regrowth in culture and karyotyping of tumors

Tumor-bearing mice were euthanized, and the tumors were excised from the flanks, dissociated by incubation with papain (500 units), vigorously triturated, and incubated for 15 min at 37°C. The cell suspension was centrifuged and resuspended in an ovomucoid protease inhibitor media solution to inhibit residual papain, followed by vigorous trituration. Cells were spun again, and the pellet was resuspended in cell culture media and plated in six-well plates. Growth and karyotyping analysis were performed as described above.

#### Growth in ultra-low adherence conditions

For this assay, 20,000 cells were plated on ultra-low attachment 24-well plates (Corning Costar). After 3 days, cells were pelleted at 250 *g* for 10 min and washed with STE buffer (100 mM NaCl, 10 mM Tris pH 7.4, 1 mM EDTA). Cells were stained with 0.4% trypan blue solution, and live cells were counted.

#### Immunofluorescence

Induced chromosome loss and control cells were plated in chamber slides, fixed with either methanol/acetone (for γH2AX) or 4% paraformaldehyde (for cleaved caspase), and stained with the primary antibodies (γH2AX—JBW301, EMD Millipore; Cleaved Caspase—#9661, Cell signaling). For measuring DNA damage in the spheres formed in low adherent conditions, the spheres were harvested as described above and treated with hypotonic 75 mM KCl

 

solution at 37°C for 15 min, and then, cytospun onto glass slides and immunofluorescence was carried out as above.

#### Blood analysis

Six-week-old mice harboring the iLoxP construct and a tamoxifen-inducible Cre recombinase expressed in long-term repopulating hematopoietic stem cells ($Id1^{IRES\text{-}creERT2}$) were injected with 16 μg of tamoxifen in corn oil over 4 days. Thirty and 80 days post-tamoxifen administration, 100 μl of tail blood was collected from these animals and stained with the hCD2 antibody (described earlier). The red blood cells were next lysed with BD FACS Lyse solution, and the remaining lymphocytes were analyzed using flow cytometry for the proportion of cells that had lost the hCD2 marker.

#### CHROM analysis

CHROM analysis on mouse chromosomes was done based on the methods described previously for human chromosomes by Davoli *et al* (2013). Briefly, the chromosomal loci for the top 300 human tumor suppressor (TSGs) and 250 oncogenes (OGs) used in their analysis were mapped to the mouse genome using the UCSC genome browser while maintaining the rankings for each gene.

#### Analysis of the human tumors from the Mitelman database

Human solid tumors that had lost (or gained) any chromosome were retrieved from the Mitelman database (http://cgap.nci.nih.gov/Chromosomes/Mitelman) and sorted according to the modal chromosome counts. This set was then stratified into either the group whose modal chromosome count was > 51 (> 2N) or the group whose modal chromosome count was between 36 and 50 (~2N). The total number of cases in each of these groups was then quantified, and the proportion of cases within the group (> 2N or ~2N) that had lost (or gained) any chromosome was calculated. For the analysis involving tumors that have lost (or gained) specific chromosomes, a similar approach was used with the exception of retrieving the tumors that have lost (or gained) the corresponding chromosome. Two-tailed two-sample *t*-test to compare sample means was used to calculate statistical significance.

**Expanded View** for this article is available online.


### Acknowledgements

The authors would like to thank Y. Zhuang for generously providing the Ch10 and Ch14 iLoxP mouse lines, Juan-Manuel Schvartzman and Dr. David Pellman (Harvard Medical School) for critical reading of the manuscript, MSKCC Flow Cytometry core facility for FACS assistance, Molecular Cytogenetics core facility for the karyotyping analysis, the Integrated Genomics Operation (IGO) core facility for the WGS and analysis, and J. Cross from the Cancer metabolism center core facility for performing the metabolite analysis. This work was supported by a grant from the Geoffrey Beene Cancer Research Center and NIH/NCI Core Grant P30 CA008748.


### Author contributions

RB and RT conceived of the experiments. RT, DHM, and RB designed the experiments. RT and YC performed the experiments. RT, DHM, and RB analyzed the data and wrote the manuscript.

### Conflict of interest

The authors declare that they have no conflict of interest.

## References


Artandi SE, Chang S, Lee SL, Alson S, Gottlieb GJ, Chin L, DePinho RA (2000) Telomere dysfunction promotes non-reciprocal translocations and epithelial cancers in mice. *Nature* 406: 641 – 645

Bakhoum SF, Kabeche L, Murnane JP, Zaki BI, Compton DA (2014) DNA-damage response during mitosis induces whole-chromosome missegregation. *Cancer Discov* 4: 1281 – 1289

Carter SL, Cibulskis K, Helman E, McKenna A, Shen H, Zack T, Laird PW, Onofrio RC, Winckler W, Weir BA, Beroukhim R, Pellman D, Levine DA, Lander ES, Meyerson M, Getz G (2012) Absolute quantification of somatic DNA alterations in human cancer. *Nat Biotechnol* 30: 413 – 421

Chen GB, Bradford WD, Seidel CW, Li R (2012) Hsp90 stress potentiates rapid cellular adaptation through induction of aneuploidy. *Nature* 482: 246 – 250

Crasta K, Ganem NJ, Dagher R, Lantermann AB, Ivanova EV, Pan Y, Nezi L, Protopopov A, Chowdhury D, Pellman D (2012) DNA breaks and chromosome pulverization from errors in mitosis. *Nature* 482: 53 – 58

Davoli T, de Lange T (2012) Telomere-driven tetraploidization occurs in human cells undergoing crisis and promotes transformation of mouse cells. *Cancer Cell* 21: 765 – 776

Davoli T, Xu AW, Mengwasser KE, Sack LM, Yoon JC, Park PJ, Elledge SJ (2013) Cumulative haploinsufficiency and triplosensitivity drive aneuploidy patterns and shape the cancer genome. *Cell* 155: 948 – 962

Davoli T, Uno H, Wooten EC, Elledge SJ (2017) Tumor aneuploidy correlates with markers of immune evasion and with reduced response to immunotherapy. *Science* 355: eaaf8399

Duijf PH, Schultz N, Benezra R (2013) Cancer cells preferentially lose small chromosomes. *Int J Cancer* 132: 2316 – 2326

Fujiwara T, Bandi M, Nitta M, Ivanova EV, Bronson RT, Pellman D (2005) Cytokinesis failure generating tetraploids promotes tumorigenesis in p53-null cells. *Nature* 437: 1043 – 1047

Gisselsson D, Pettersson L, Hoglund M, Heidenblad M, Gorunova L, Wiegant J, Mertens F, Dal Cin P, Mitelman F, Mandahl N (2000) Chromosomal breakage-fusion-bridge events cause genetic intratumor heterogeneity. *Proc Natl Acad Sci USA* 97: 5357 – 5362

Gregoire D, Kmita M (2008) Recombination between inverted loxP sites is cytotoxic for proliferating cells and provides a simple tool for conditional cell ablation. *Proc Natl Acad Sci USA* 105: 14492 – 14496

Guadamillas MC, Cerezo A, del Pozo MA (2011) Overcoming anoikis - pathways to anchorage-independent growth in cancer. *J Cell Sci* 124: 3189 – 3197

Hein J, Boichuk S, Wu J, Cheng Y, Freire R, Jat PS, Roberts TM, Gjoerup OV (2009) Simian virus 40 large T antigen disrupts genome integrity and activates a DNA damage response via Bub1 binding. *J Virol* 83: 117 – 127

Jankovic V, Ciarrocchi A, Boccuni P, DeBlasio T, Benezra R, Nimer SD (2007) Id1 restrains myeloid commitment, maintaining the self-renewal capacity of hematopoietic stem cells. *Proc Natl Acad Sci USA* 104: 1260 – 1265

Janssen A, van der Burg M, Szuhai K, Kops GJ, Medema RH (2011) Chromosome segregation errors as a cause of DNA damage and structural chromosome aberrations. *Science* 333: 1895 – 1898

Kamijo T, Zindy F, Roussel MF, Quelle DE, Downing JR, Ashmun RA, Grosveld G, Sherr CJ (1997) Tumor suppression at the mouse INK4a locus mediated by the alternative reading frame product p19ARF. *Cell* 91: 649 – 659

Laughney AM, Elizalde S, Genovese G, Bakhoum SF (2015) Dynamics of tumor heterogeneity derived from clonal karyotypic evolution. *Cell Rep* 12: 809 – 820

Lewandoski M, Martin GR (1997) Cre-mediated chromosome loss in mice. *Nat Genet* 17: 223 – 225

Lionnet T, Czaplinski K, Darzacq X, Shav-Tal Y, Wells AL, Chao JA, Park HY, de Turris V, Lopez-Jones M, Singer RH (2011) A transgenic mouse for *in vivo* detection of endogenous labeled mRNA. *Nat Methods* 8: 165 – 170

Maciejowski J, Li YL, Bosco N, Campbell PJ, de Lange T (2015) Chromothripsis and kataegis induced by telomere crisis. *Cell* 163: 1641 – 1654

Nam HS, Benezra R (2009) High levels of Id1 expression define B1 type adult neural stem cells. *Cell Stem Cell* 5: 515 – 526

Nicholson JM, Macedo JC, Mattingly AJ, Wangsa D, Camps J, Lima V, Gomes AM, Doria S, Ried T, Logarinho E, Cimini D (2015) Chromosome mis-segregation and cytokinesis failure in trisomic human cells. *Elife* 4: e05068

Oromendia AB, Dodgson SE, Amon A (2012) Aneuploidy causes proteotoxic stress in yeast. *Genes Dev* 26: 2696 – 2708

Passerini V, Ozeri-Galai E, de Pagter MS, Donnelly N, Schmalbrock S, Kloosterman WP, Kerem B, Storchova Z (2016) The presence of extra chromosomes leads to genomic instability. *Nat Commun* 7: 10754

Pfau SJ, Silberman RE, Knouse KA, Amon A (2016) Aneuploidy impairs hematopoietic stem cell fitness and is selected against in regenerating tissues *in vivo*. *Genes Dev* 30: 1395 – 1408

Randle DH, Zindy F, Sherr CJ, Roussel MF (2001) Differential effects of p19(Arf) and p16(Ink4a) loss on senescence of murine bone marrow-derived preB cells and macrophages. *Proc Natl Acad Sci USA* 98: 9654 – 9659

Schvartzman JM, Sotillo R, Benezra R (2010) Mitotic chromosomal instability and cancer: mouse modelling of the human disease. *Nat Rev Cancer* 10: 102 – 115

Selvarajah S, Yoshimoto M, Park PC, Maire G, Paderova J, Bayani J, Lim G, Al-Romaih K, Squire JA, Zielenska M (2006) The breakage-fusion-bridge (BFB) cycle as a mechanism for generating genetic heterogeneity in osteosarcoma. *Chromosoma* 115: 459 – 467

Sheltzer JM, Blank HM, Pfau SJ, Tange Y, George BM, Humpton TJ, Brito IL, Hiraoka Y, Niwa O, Amon A (2011) Aneuploidy drives genomic instability in yeast. *Science* 333: 1026 – 1030

Sheltzer JM, Ko JH, Replogle JM, Habibe Burgos NC, Chung ES, Meehl CM, Sayles NM, Passerini V, Storchova Z, Amon A (2017) Single-chromosome gains commonly function as tumor suppressors. *Cancer Cell* 31: 240 – 255

Simon JE, Bakker B, Foijer F (2015) CINcere modelling: what have mouse models for chromosome instability taught us? *Recent Results Cancer Res* 200: 39 – 60

Sotillo R, Hernando E, Diaz-Rodriguez E, Teruya-Feldstein J, Cordon-Cardo C, Lowe SW, Benezra R (2007) Mad2 overexpression promotes aneuploidy and tumorigenesis in mice. *Cancer Cell* 11: 9 – 23

Stingele S, Stoehr G, Peplowska K, Cox J, Mann M, Storchova Z (2012) Global analysis of genome, transcriptome and proteome reveals the response to aneuploidy in human cells. *Mol Syst Biol* 8: 608

Tang YC, Williams BR, Siegel JJ, Amon A (2011) Identification of aneuploidy-selective antiproliferation compounds. *Cell* 144: 499 – 512

Torres EM, Sokolsky T, Tucker CM, Chan LY, Boselli M, Dunham MJ, Amon A (2007) Effects of aneuploidy on cellular physiology and cell division in haploid yeast. *Science* 317: 916 – 924

Williams BR, Prabhu VR, Hunter KE, Glazier CM, Whittaker CA, Housman DE, Amon A (2008) Aneuploidy affects proliferation and spontaneous immortalization in mammalian cells. *Science* 322: 703 – 709

Zhang M, Cheng L, Jia Y, Liu G, Li C, Song S, Bradley A, Huang Y (2016) Aneuploid embryonic stem cells exhibit impaired differentiation and increased neoplastic potential. *EMBO J* 35: 2285 – 2300

Zhu Y, Kim YM, Li S, Zhuang Y (2010) Generation and analysis of partially haploid cells with Cre-mediated chromosome deletion in the lymphoid system. *J Biol Chem* 285: 26005 – 26012

Zindy F, Quelle DE, Roussel MF, Sherr CJ (1997) Expression of the p16INK4a tumor suppressor versus other INK4 family members during mouse development and aging. *Oncogene* 15: 203 – 211

 